Claudin-low-like mouse mammary tumors show distinct transcriptomic patterns uncoupled from genomic drivers

Christian Fougner[1], Helga Bergholtz[1], Raoul Kuiper[2], Jens Henrik Norum[1] and Therese Sørlie[1, 3, 4]

1. Department of Cancer Genetics, Oslo University Hospital, Oslo, Norway

2. Department of Laboratory Medicine, Karolinska Institutet, Stockholm, Sweden

3. Centre for Cancer Biomarkers CCBIO, University of Bergen, Norway

4. Institute for Clinical Medicine, University of Oslo, Norway.

Abstract

Claudin-low breast cancer is a molecular subtype associated with poor prognosis and without targeted treatment options. The claudin-low subtype is defined by certain biological characteristics, some of which may be clinically actionable, such as high immunogenicity. In mice, the medroxyprogesterone acetate (MPA) and 7,12-dimethylbenzanthracene (DMBA) induced mammary tumor model yields a heterogeneous set of tumors, a subset of which display claudin-low features. Neither the genomic characteristics of MPA/DMBA-induced claudin-low tumors, nor those of human claudin-low breast tumors, have been thoroughly explored.

The transcriptomic characteristics and subtypes of MPA/DMBA-induced mouse mammary tumors were determined using gene expression microarrays. Somatic mutations and copy number aberrations in MPA/DMBA-induced tumors were identified from whole exome sequencing data. A publicly available dataset was queried to explore the genomic characteristics of human claudin-low breast cancer and to validate findings in the murine tumors.

Half of MPA/DMBA-induced tumors showed a claudin-low-like subtype. All tumors carried mutations in known driver genes. While the specific genes carrying mutations varied between tumors, there was a consistent mutational signature with an overweight of T>A transversions in TG dinucleotides. Most tumors carried copy number aberrations with a potential oncogenic driver effect. Overall, several genomic events were observed recurrently, however none accurately delineated claudin-low-like tumors. Human claudin-low breast cancers carried a distinct set of genomic characteristics, in particular a relatively low burden of mutations and copy number aberrations. The gene expression characteristics of claudin-low-like MPA/DMBA-induced tumors accurately reflected those of human claudin-low tumors, including epithelial-mesenchymal transition phenotype, high level of immune activation and low degree of differentiation. There was an elevated expression of the immunosuppressive

genes *PTGS2* (encoding COX-2) and *CD274* (encoding PD-L1) in human and murine claudin-low tumors. Our findings show that the claudin-low breast cancer subtype is not demarcated by specific genomic aberrations, but carries potentially targetable characteristics warranting further research.

Author Summary

Breast cancer is comprised of several distinct disease subtypes with different etiologies, prognoses and therapeutic targets. The claudin-low breast cancer subtype is relatively poorly understood, and no specific treatment exists targeting its unique characteristics. Animal models accurately representing human disease counterparts are vital for developing novel therapeutics, but for the claudin-low breast cancer subtype, no such uniform model exists. Here, we show that exposing mice to the carcinogen DMBA and the hormone MPA causes a diverse range of mammary tumors to grow, and half of these have a gene expression pattern similar to that seen in human claudin-low breast cancer. These tumors have numerous changes in their DNA, with clear differences between each tumor, however no specific DNA aberrations clearly demarcate the claudin-low subtype. We also analyzed human breast cancers and show that human claudin-low tumors have several clear patterns in their DNA aberrations, but no specific features accurately distinguish claudin-low from non-claudin-low breast cancer. Finally, we show that both human and murine claudin-low tumors express high levels of genes associated with suppression of immune response. In sum, we highlight claudin-low breast cancer as a clinically relevant subtype with a complex etiology, and with potential unexploited therapeutic targets.

Introduction

The claudin-low subtype of breast cancer (BC) is a distinct disease entity associated with a relatively poor prognosis, and with an inadequately understood clinical significance [1–3]. It is characterized by low expression of tight junction and cell-cell adhesion genes, low degree of differentiation, epithelial-mesenchymal transition (EMT) phenotype and high level of immune cell infiltration [2]. The claudin-low subtype represents 7-14% of all breast cancers, and despite its unique biological features, there are no therapies specifically targeting the subtype [2–5]. While claudin-low tumors are found in several large scale studies, there is a paucity of information regarding their specific genomic characteristics [6–9]. Thus, significant gaps remain in the understanding of the biology of claudin-low tumors, and there is a need for further research to explore how their unique features may be therapeutically targeted.

Accurate preclinical models are vital for research into novel treatment options. Mouse mammary tumors may be induced through exposure to medroxyprogesterone acetate (MPA) and 7,12-dimethylbenzanthracene (DMBA) [10]. The tumors generated by this protocol are diverse, and a subset of these show similarities to the human claudin-low subtype [11,12]. A homogeneous primary *in vivo* model of claudin-low breast cancer does not currently exist [11]. While the mechanisms of MPA [10,13] and DMBA [14–17] have been described, there is still contention regarding the suitability of a chemically induced model of cancer for a disease that is not primarily caused by carcinogens in humans [18]. Evaluating the claudin-low subset of MPA/DMBA-induced tumors as a model for human disease is therefore an important step toward advancing preclinical research of claudin-low breast cancer.

In this study, we identified and comprehensively characterized claudin-low-like mouse mammary tumors generated by MPA/DMBA-induced carcinogenesis. Through genomic and transcriptomic analyses, we evaluated these tumors as a model for human claudin-low breast cancer and showed these tumors to be phenotypically accurate representations of their human

89 counterparts. In parallel, we analyzed the previously unexplored genomic features of human
90 claudin-low breast cancer. Our findings highlighted several features of claudin-low breast
91 cancer with potential therapeutic implications, including a low tumor mutational burden, high
92 expression of the immune checkpoint gene *CD274* (encoding PD-L1) and high expression of
93 *PTGS2* (encoding cyclooxygenase-2).
94
95

Results

Gene expression subtyping reveals two distinct tumor clusters

We determined the murine transcriptomic subtypes of 17 MPA/DMBA-induced mammary tumors from 13 mice (S1 File) by performing a hierarchical clustering of gene expression data using the mouse intrinsic gene list [11]. This revealed nine murine subtypes in the cohort (Fig 1, Table 1, S2 File). The tumors separated into two distinct clusters. One cluster consisted of claudin-low^{Ex} and squamous-like^{Ex} tumors, both of which have been shown to resemble the human claudin-low subtype [11]; this is therefore referred to as the claudin-low-like cluster. The other cluster contained tumors from seven different subtypes and is referred to as the mixed cluster. In four instances, two tumors from different mammary glands were harvested from the same mouse. These were classified as different subtypes in all cases and are presumed to be distinct primary tumors. All normal mammary gland samples were classified as normal-like^{Ex}, and clustered separately from the tumors.

Table 1: Subtype distribution of MPA/DMBA-induced tumors and normal mouse mammary gland tissue

No. of samples	Murine subtype	Cluster
6	Claudin-low^{Ex}	Claudin-low-like
2	Squamous-like^{Ex}	Claudin-low-like
3	PyMT^{Ex}	Mixed
1	Class3^{Ex}	Mixed
1	Class8^{Ex}	Mixed
1	Class14^{Ex}	Mixed
1	Erbb2-like^{Ex}	Mixed
1	Wnt1-Early^{Ex}	Mixed
1	Wnt1-Late^{Ex}	Mixed
5 (normal mammary)	Normal^{Ex}	Normal

Histopathological analysis corroborated the intertumor heterogeneity that was demonstrated by subtyping (S1 File). Five of the eight claudin-low-like tumors, including both squamous-

114 like^{Ex} tumors, showed a squamous appearance, while no tumors in the mixed cluster displayed
115 this histological phenotype (p = 0.009, Fisher's exact test). There was also a higher frequency
116 of claudin-low-like tumors showing marked neutrophil infiltration (p = 0.002, Fisher's exact
117 test) and displaying a marked or partial spindloid appearance (p = 0.050, Fisher's exact test)
118 compared to tumors in the mixed cluster.

119 Mutations in MPA/DMBA-induced mammary tumors are independent of gene 120 expression subtype

121 To determine the genetic characteristics of the tumors, we performed exome sequencing to a
122 mean depth of 58, with 84% of bases being sequenced to a coverage of 20x or higher. We
123 identified a mean of 589 mutations per tumor (range: 288 to 1795), corresponding to a mean
124 mutation rate of 11.9 mutations per megabase (range: 5.8 to 36.2) (Fig 2B). This is
125 substantially higher than the average 1.3 mutations per megabase found in human breast
126 cancer [19]. There was no significant difference in mutational burden between the tumors in
127 the claudin-low-like and the mixed cluster, and the only subtype specific trend was a
128 particularly high mutational burden in the two squamous-like^{Ex} tumors (Fig 2B).

129 All tumors carried mutations in driver genes defined by the COSMIC cancer gene census list
130 [20], with a mean of 13.8 driver genes carrying mutations per tumor (range: 4 to 29) (Fig 2A).
131 Several driver genes were recurrently mutated, including *Trp53*, *Kras*, and *Kmt2c* (S3 File),
132 but no driver genes carried mutations at a significantly different rate between the two clusters.
133 We did, however, identify two notable trends which did not reach statistical significance: an
134 elevated rate of *Trp53* mutations in the claudin-low-like cluster (50% vs. 11%, p = 0.13, two-
135 tailed Fisher's exact test) and an elevated rate of *Zfhx3* mutations also in the claudin-low-like
136 cluster (37.5% vs. 0%, p = 0.08, two-tailed Fisher's exact test). No mutations were
137 significantly associated with histological features.

138 ## MPA/DMBA-induced tumors and human breast cancers display disparate gene
139 ## mutational profiles

140 To narrow down potential driver mutations in the MPA/DMBA-induced tumors, we
141 compared amino acid changes caused by mutations in driver genes to known amino acid
142 changes in human cancers [20] (Table 2, S4 File). There were hotspot amino acid changes in
143 all *Ras* genes, including *Kras* G12C, G13R, Q61H, *Hras* Q61L and *Nras* Q61L. In total, 8 of
144 18 tumors carried hotspot amino acid changes in *Ras* genes. There was one *Pik3ca* mutation
145 in the cohort causing an H1047R amino acid change. This mutation is frequently found in
146 human breast cancer and has previously been reported in DMBA-induced mouse mammary
147 tumors [21].

148 **Table 2. Selected hotspot mutations in MPA/DMBA-induced tumors**
149

Sample	Gene	Amino acid change
S176_14_2	*Ctnnb1*	Asp32Asn
S416_15_2	*Ctnnb1*	Thr41Ile
S187_14_1	*Hras*	Gln61Leu
S412_15_2	*Hras*	Gln61Leu
S159_14_8	*Kras*	Gly12Cys
S160_14_2	*Kras*	Gly12Cys
S176_14_2	*Kras*	Gly13Arg
S189_14_2	*Kras*	Gln61His
S153_14_2	*Nras*	Gln61Leu
S416_15_9	*Nras*	Gln61Leu
S187_14_1	*Pik3ca*	His1047Arg
S132_14_5	*Trp53*	His211Pro
S153_14_2	*Trp53*	Lys129Met
S400_15_2	*Trp53*	Gln141Pro
S400_15_2	*Trp53*	His211Pro

150

151 There were marked disparities between the gene mutational profiles of human breast cancer
152 [22] and MPA/DMBA-induced tumors (Fig 2C, S5 File). The two most frequently mutated
153 genes in breast cancer are *PIK3CA* and *TP53*. While *TP53* showed comparable mutation rates
154 between human breast cancer and MPA/DMBA-induced tumors (34% and 28%,
155 respectively), *PIK3CA* mutation does not appear to be a common event in MPA/DMBA-

156 induced tumors (35% in BC, 6% in MPA/DMBA). Several frequently mutated genes in breast
157 cancer, such as *CDH1*, *GATA3* and *MAP3K1,* were not mutated in any MPA/DMBA-induced
158 tumors. Conversely, many genes frequently mutated in MPA/DMBA-induced tumors, such as
159 *ATR*, *FAT1* and *KRAS*, are rarely mutated in breast cancer.

160 DMBA induces a characteristic mutational spectrum with a high frequency of 161 T>A transversions in TG dinucleotides

162 To characterize the mutagenic profile of DMBA, we analyzed the mutational spectra of the
163 MPA/DMBA-induced tumors. Mutations showed a majority of T>A transversions, which
164 accounted for 63% of all mutations (S1A Fig). In their trinucleotide context, thymine
165 mutations (T>N) were overrepresented in positions with a 3' guanine nucleotide (S1B & S1C
166 Fig, S6 File). This was statistically significant when compared to the proportion of thymine
167 nucleotides in an NTG context in the mouse reference genome ($p < 0.001$ in all cases, two-
168 tailed Wilcoxon rank-sum test). There was a similar overrepresentation of cytosine mutations
169 in positions with a 3' adenine. This was statistically significant for C>A and C>G mutations
170 ($p < 0.001$), but not for C>T mutations ($p = 0.089$), when compared to the proportion of
171 cytosine nucleotides in an NCA context in the mouse reference genome.

172 Mutation signature analysis revealed evidence of signatures 4, 6, 22, 24 and 25 [23] in the
173 MPA/DMBA-induced tumors (S1D Fig). All tumors were associated with signature 22, while
174 signatures 4 and 25 were found in 17 and 11 of the 18 tumors, respectively. Signatures 24 and
175 6 were only found in four and one tumor(s), respectively. Notably, none of the signatures
176 found in MPA/DMBA-induced tumors have been associated with human breast cancer [23].

177 MPA/DMBA-induced tumors have diverse copy number profiles

178 Breast cancer is largely driven by copy number aberrations (CNAs) [24], yet the copy number
179 profiles of MPA/DMBA-induced mammary tumors have not previously been described. We
180 found a mean of 1299 genes with CNA per tumor (range: 90 – 3057), of which a mean of

181 65% were amplifications. There was a tendency for claudin-low-like tumors to have a lower
182 burden of CNAs, with a mean of 919 genes carrying CNA, compared to the mixed group of
183 tumors, with a mean of 1637 genes carrying CNA (Fig 3A). This trend did however not reach
184 statistical significance ($p = 0.139$, two-tailed Wilcoxon rank-sum test).

185 To determine CNAs in the MPA/DMBA-induced tumors with a potential oncogenic driver
186 effect, we identified amplifications and deletions known to be associated with cancer [20]
187 (Fig 3B*)*. We found that 14 of the 18 tumors carried potential driver CNAs (range: 0 to 4,
188 mean: 2.6). Three of the four tumors not carrying potential driver CNAs were claudin-low-
189 like. There was however no statistically significant difference in the number of potential
190 driver CNAs between the clusters. Several genes had recurrent CNAs, but none occurred at a
191 statistically significant different rate in one cluster versus the other.

192 Only two of the CNA events identified in MPA/DMBA-induced tumors occur at a notable
193 rate in human breast cancer; *Mdm4* is amplified in 25% and *Ppm1d* is amplified in 10% of
194 human BC [6,7].

195 We observed two sets of tumors carrying remarkably similar CNA profiles (Fig 3B). None of
196 the tumors in these two sets displayed the same murine subtype as any other tumor within the
197 same set.

198 The human claudin-low breast cancer genome is characterized by a low 199 mutational burden, frequent *TP53* mutations and a low rate of CNA

200 Little has been published specifically describing the genomic characteristics of human
201 claudin-low breast cancer. We therefore analyzed the 218 claudin-low tumors found in the
202 METABRIC dataset, for which DNA sequence data from 173 genes and whole genome copy
203 number data is available [6,7].

204 Claudin-low tumors, with a mean of 4.7 mutations per tumor, carried relatively few mutations
205 compared to all other tumors, with a mean of 7.3 mutations per tumor ($p < 0.001$, two-tailed

206 Wilcoxon rank-sum test) (Fig 4A). Claudin-low tumors share several characteristics with
207 basal-like tumors and are often classified as such by the PAM50 assay [6,7,25]; however,
208 basal-like tumors showed a significantly higher mutational burden than claudin-low tumors
209 (mean: 8.08 mutations per tumor, $p < 0.001$, two-tailed Wilcoxon rank-sum test).

210 There was a high degree of overlap between the genes most frequently mutated in claudin-low
211 breast cancers and the genes most frequently mutated in all other breast cancers (Fig 4B).
212 Most of these genes carried mutations at similar rates between claudin-low and non-claudin-
213 low tumors, albeit with a tendency towards a slightly lower rate in claudin-low tumors. There
214 were however two notable differences in mutational frequency: a significantly higher rate of
215 *TP53* mutations and a significantly lower rate of *PIK3CA* mutations in claudin-low tumors
216 compared to other tumors. Similarly, basal-like tumors also carried a high frequency of *TP53*
217 mutations and a low frequency of *PIK3CA* mutations [7,22].

218 Human claudin-low breast tumors carried significantly fewer genes with copy number
219 aberration (mean: 4879) compared to all other tumors (mean: 6247; $p < 0.001$, two-tailed
220 Wilcoxon rank-sum test) (Fig 4C). This difference was also marked when comparing claudin-
221 low tumors with basal like tumors (mean: 10175 genes per tumor; $p < 0.001$, two-tailed
222 Wilcoxon rank-sum test).

223 By gene, the most frequent copy number event in claudin-low breast cancer was *MYC*
224 amplification, found in 20% of cases (Fig 4D). In comparison, this event was found in 26% of
225 all other breast tumors. The ten most frequently amplified genes in claudin-low breast cancer
226 were all located at chromosomal position 8q24, a region also frequently amplified in basal-
227 like breast cancers [6,7].

228 **Claudin-low-like MPA/DMBA-induced mammary tumors accurately reflect the**
229 **gene expression characteristics of their human counterpart**

230 We explored several established gene expression features of the claudin-low subtype and
231 found that MPA/DMBA-induced claudin-low-like tumors accurately mirrored their human
232 counterpart. Specifically, claudin-low-like tumors had low expression of genes involved in
233 cell-cell adhesion, low expression of luminal genes, and high expression of genes related to
234 EMT (Fig 5A, S2 Fig). Claudin-low-like tumors also showed a markedly lower degree of
235 differentiation compared to tumors in the mixed cluster. In particular, the claudin-low-like
236 cluster expressed significantly higher and lower levels of *Cd44* and *Cd24a*, respectively,
237 indicating a stem cell-like phenotype in these tumors [25,26] (S3 Fig). There was no
238 significant difference in the expression of proliferation-related genes between the two
239 clusters. Vascular content-related genes were expressed at a significantly higher level in
240 claudin-low-like tumors compared to the tumors in the mixed cluster (S2 Fig), indicating a
241 higher degree of neoangiogenesis in these tumors.

242 Immune cell admixture was significantly higher in the claudin-low-like tumors compared to
243 tumors in the mixed cluster ($p < 0.001$, two-tailed Wilcoxon rank-sum test) and compared to
244 normal mammary gland samples ($p = 0.006$). We also found higher expression of genes
245 related to immunosuppression and interferons in the claudin-low-like cluster compared to
246 both the mixed cluster and normal mammary gland samples. High immune cell infiltration
247 combined with high expression of type 1 interferon-related and immunosuppressive genes are
248 characteristics of tumors that may respond to immunotherapeutics [27,28].

249 We identified a significantly elevated expression of two potentially actionable genes related to
250 immunosuppression in the claudin-low-like tumors: the immune checkpoint encoding gene
251 *Cd274* and the cyclooxygenase encoding gene *Ptgs2* (Fig 5B). These features were also
252 characteristic of human claudin-low tumors in the METABRIC cohort [6,7], which showed
253 significantly higher expression levels of both *PTGS2* and *CD274* compared to non-claudin-

low breast tumors ($p < 0.001$ for both, two-tailed Wilcoxon rank-sum test), and compared specifically to basal-like tumors ($p = 0.004$ and $p < 0.001$, respectively) (Fig 5C). These characteristics may indicate a susceptibility to immune checkpoint inhibitors and cyclooxygenase inhibitors in human claudin-low breast cancer [29,30].

Discussion

In this study, we have performed a comprehensive analysis of mutations, copy number aberrations and gene expression characteristics of MPA/DMBA-induced tumors. We found marked inter-tumor heterogeneity, and showed that half of the tumors displayed a claudin-low-like phenotype, in line with a previous report [11]. Our findings demonstrate that these tumors provide a transcriptomically accurate representation of human claudin-low breast tumors, reflecting key features such as an EMT phenotype, high level of immune infiltration and a low degree of differentiation.

MPA/DMBA-induced tumors carried a mutational burden multiple times that of human breast cancer, a high frequency of activating *Ras*-mutations and a characteristic mutational spectrum. The specific genes carrying mutations varied widely between tumors, however all tumors had a consistent mutational signature. This indicates that the dominant mutational process in these tumors is DMBA-induced mutagenesis, and not aberrations occurring after tumor initiation, as a result of e.g. disrupted DNA-repair. Copy number aberrations in MPA/DMBA-induced tumors have not previously been explored, and we show here that most tumors carry potential driver CNAs. However, while we noted several genomic trends, such as a higher rate of *Trp53* mutation and a lower burden of CNA in MPA/DMBA-induced claudin-low-like tumors, no individual genomic features accurately delineated the two gene expression-based tumor clusters. Further, several tumors carried similar sets of mutations and/or CNAs but displayed different subtypes. This suggests that no specific genomic event determines tumor subtype, and that other etiological models may be more appropriate, such as different cells-of-origin [31] or microenvironmental factors [32]. This finding concurs with recent reports showing that transgenic mouse mammary tumors display histological and transcriptomic phenotypes largely uncoupled from their underlying driver mutations [33,34]. One possible model for MPA/DMBA-induced tumorigenesis is therefore as follows: first, MPA induces a RANK-l mediated mammary gland proliferation [10,13]. DMBA then induces

286 mutations in mammary cells in a pattern as elucidated by our mutation signature analysis,
287 predominantly in TG and CA dinucleotides, stochastically distributed throughout the genome.
288 The tumor is initiated when one or more driver mutations occur, for example *Trp53* or *Ras*-
289 mutation, with the tumor phenotype, however, determined by non-genomic factors. The
290 biochemical mechanism of DMBA-induced mutagenesis has been described [14,15], whereas
291 no causal mechanism for DMBA-induced copy number aberration is known; it is therefore
292 likely that CNAs arise after tumor initiation.

293 Previous genomic analyses which included human claudin-low breast tumors have either not
294 included specific analyses of the subtype [6,7], included few samples [3], or have been
295 restricted to the triple-negative [35,36] or metaplastic [37] subsets of claudin-low tumors. We
296 show here that human claudin-low tumors are characterized by a low number of mutations
297 and a low burden of CNAs. This finding is surprising, given the apparent inverse correlation
298 between CNA and mutational burden in cancer [24], and indicates that the claudin-low
299 subtype is relatively genomically stable compared to other breast cancers. We also find
300 similarities in genomic characteristics between claudin-low tumors and basal-like tumors, in
301 particular a high frequency of *TP53* mutations, a low frequency of *PIK3CA* mutations, and
302 8q24 amplifications as a common event. While the transcriptomic similarity between these
303 two subtypes is established [25], these findings illustrate that there are also marked genomic
304 similarities between claudin-low and basal breast cancer, albeit with a lower burden of
305 genomic aberrations in claudin-low tumors.

306 Claudin-low tumors show high expression of immune-related genes and a high level of
307 immune cell infiltration [3,25,38]. However, claudin-low tumors also express high levels of
308 immunosuppressive genes. In MPA/DMBA-induced claudin-low-like tumors, we observed an
309 elevated expression of two particularly notable genes involved in immunosuppression: *Ptgs2*
310 (encoding COX-2) and *Cd274* (encoding PD-L1). This observation was consistent in human
311 claudin-low breast cancer. COX-2 may be implicated in cancer development through several

312 mechanisms: reducing apoptosis, increasing epithelial cell proliferation, promoting
313 angiogenesis, increasing invasiveness of tumor cells and immunosuppression [39–41]. COX-2
314 may also be involved in vasculogenic mimicry, a process in which epithelial tumor cells form
315 vascular channel-like structures without participation of endothelial cells, allowing nutrients
316 to reach tumor cells without the need for neoangiogenesis [42]. Vasculogenic mimicry has
317 previously been shown to occur in claudin-low tumors [43]. COX-2 and PD-L1 are clinically
318 actionable through the use of COX-inhibitors [29] and checkpoint inhibitors [44],
319 respectively. Further research into the potential use of checkpoint inhibitors and COX-
320 inhibitors in claudin-low breast cancer is warranted, with promising future avenues including
321 combinatorial Treg-depletion [38].

322 In summary, we have found that claudin-low-like MPA/DMBA-induced mouse mammary
323 tumors are a transcriptomically accurate model for human claudin-low breast cancer. We did
324 not find strong evidence that claudin-low-like MPA/DMBA-induced tumors are delineated by
325 any specific genomic features, however the relatively small number of samples included in
326 this study may have obscured possible associations. By analyzing publicly available data, we
327 showed that human claudin-low breast cancer is a relatively genomically stable subtype.
328 There is a high expression of genes related to immunosuppression in claudin-low breast
329 cancers, a feature which is evident in claudin-low-like MPA/DMBA-induced tumors. Our
330 observations suggest immunosuppression as a potential therapeutic target in claudin-low
331 breast cancer and indicate MPA/DMBA-induced claudin-low-like tumors as an appropriate
332 model for continued research.
333
334

Material and Methods

Ethics statement

The Norwegian Food Safety Authority approved all experiments in advance of their implementation (FOTS ID #4385). All mice were bred and maintained within a specific pathogen free (SPF) barrier facility according to local and national regulations, with food and water *ad libitum*. For invasive procedures, animals were anaesthetized with sevoflurane gas. Animals were euthanized by cervical dislocation under anesthesia with sevoflurane gas.

Mouse strains and tumor induction

Animals from an Lgr5-creERT2-EGFP;Rb/C transgenic mouse strain on a pure FVB/N background were purchased from Jackson Laboratory (www.jax.org), kindly gifted from Rune Toftgård (*Karolinska Institutet*, Sweden) and locally bred. The transgenes are considered biologically inert, and offspring from all potential genotypes were used (wildtype, single transgene and double transgene). Female mice were treated with medroxyprogesterone acetate (MPA) and 7,12-dimethylbenzanthracene (DMBA) in accordance with established protocol [10]. In brief: 90-day release MPA pellets (50 mg/pellet, Innovative Research of America cat.# NP-161) were implanted subcutaneously at 6 and 19 weeks after birth. 1 mg DMBA (Sigma Aldrich cat.# D3254) dissolved in corn oil (Sigma Aldrich cat.# C8267) was administered by oral gavage at 9, 10, 12 and 13 weeks after birth. Tumor growth was regularly monitored by manual palpation and measured by caliper. Tumor volume was estimated using the following formula: volume = (width^2 * length)/2. When the tumors reached the maximum allowed size of 1000mm^3, or at the age of 32 weeks, tissue was collected at necropsy and fixed in 4% paraformaldehyde (PFA) or snap frozen and stored at -80 °C. 18 tumors from 14 mice, of which four mice carried two mammary tumors, were subject to genomic and transcriptomic analyses. Six normal mammary glands collected from

359 mice not undergoing MPA/DMBA-treatment were included as controls. Mouse features and
360 histopathological tumor features, can be found in S1 File.

361 Histopathology and immunohistochemistry

362 Mouse tissue was fixed overnight in 4% PFA, routinely processed and paraffin embedded.
363 Formalin-fixed paraffin-embedded tissue was sectioned and stained with hematoxylin and
364 eosin (HE). HE-stained tissue was classified by a certified veterinary pathologist.
365 Immunohistochemical staining was performed as previously described [45] with primary
366 antibodies against K5 (Covance cat.# PRB-160P), K18 (Progen cat.# 61028), Ki67
367 (Novocastra cat.# NCL-Ki67p), ERα (Millipore cat.# 06-935), PR (Abcam cat.# ab131486)
368 and Her2/Erbb2 (Millipore cat.# 06-562).

369 DNA and RNA isolation

370 DNA isolation for exome sequencing was carried out at Theragen Etex Bio Institute (Seoul,
371 South Korea). DNA was isolated using QIAamp DNA Mini Kit (Qiagen cat.# 51306) per
372 manufacturer's protocol. DNA from two samples (*S159_14_11* and *S176_14_11*) was isolated
373 using CTAB Extraction Solution (Biosesang cat.# C2007) per manufacturer's protocol. DNA
374 integrity was assessed by electrophoresis and concentration was determined using the
375 Nanodrop ND-1000 spectrophotometer (Thermo Scientific cat.# ND-1000) and Qubit
376 fluorometer (Thermo Scientific cat.# Q33226). Total RNA and DNA isolation for gene
377 expression microarrays was carried out using the QIAcube system (Qiagen cat.# 9001292)
378 with the AllPrep DNA/RNA Universal Kit (Qiagen cat.# 80224) according to the protocol
379 provided by the supplier, with 30mg tissue as input. The tissue was manually minced with a
380 scalpel on ice followed by lysis and homogenization using TissueLyzer LT (Qiagen cat.#
381 85600) and Qiashredder (Qiagen cat.# 79654), respectively. Nucleic acid concentrations were
382 measured by NanoDrop ND-1000 spectrophotometer and RNA integrity was analyzed using
383 Agilent 2100 Bioanalyzer (Agilent Technologies cat.# G2939BA).

384 ## Gene expression microarrays

385 Gene expression profiling was performed using RNA isolated from eighteen snap frozen
386 MPA/DMBA-induced tumors and six normal/untreated mouse mammary gland samples.
387 Whole genome expression data was obtained using Agilent Sureprint G3 Mouse Gene
388 Expression 8x60K microarrays (Agilent Technologies cat.# G4852B) with Low Input Quick
389 Amp Labeling protocol (Agilent Technologies cat.# 5190-2331) and the Cy3 fluorophore.
390 40ng RNA was used for input. Microarrays were scanned using an Agilent SureScan
391 Microarray Scanner (Agilent Technologies cat.# G4900DA) and data was extracted using
392 Agilent Feature Extraction software. One tumor sample (*S422_15_2*) failed quality control
393 and was excluded from further gene expression analyses.

394 ## Gene expression analyses

395 Gene expression data was analyzed using Qlucore Omics Explorer 3.2 (Qlucore AB) and R
396 version 3.3.2 [46]. Gene expression values were quantile normalized and probes with a
397 standard deviation of less than 2.8% of the largest observed standard deviation were filtered
398 out. For genes represented by more than one probe, mean expression values were calculated
399 to obtain one gene expression value per gene. Principal component analysis was performed to
400 assess data quality and one normal mammary gland sample (*S178_14_2*) was identified as an
401 outlier and removed from further analysis. Murine subtypes were determined by first
402 calculating centroids for each subtype using the original data from the mouse intrinsic gene
403 list [11], followed by calculating Spearman correlation for every sample to each of the
404 subtype centroids. The subtype with the highest correlation coefficient was assigned as the
405 sample's subtype.

406 Unsupervised hierarchical clustering was performed using average linkage and Spearman
407 correlation as the distance metric. Immune cell infiltration was inferred using ESTIMATE
408 [47]. Scores for gene signatures relevant to the claudin-low subtype (adhesion, EMT,

409 luminalness, proliferation, vascular content, immunosuppression and interferons [25,43,48–
410 50]) were calculated using a standard (Z) score approach: for every gene in each signature, a
411 standardized expression value was calculated by subtracting the mean across all samples, then
412 dividing by the standard deviation. Calculation of the mean of the standardized expression
413 values across all genes in the signature yielded the score. Gene lists included in the different
414 signatures are found in S7 File. The degree of differentiation was calculated using a
415 differentiation predictor [25]. Two-tailed Wilcoxon rank-sum tests were used for statistical
416 testing of differences in scores between two groups.

417 **Whole exome sequencing**

418 Whole exome sequencing was carried out at Theragen Etex Bio Institute. Library preparation
419 and target enrichment was carried out using the SureSelect XT Mouse All Exon Kit (Agilent
420 cat.# 5190-4641) per manufacturer's instructions. Sequencing was performed on an Illumina
421 HiSeq 2500 (Illumina cat.# SY–401–2501). DNA was sequenced to an average depth of 58.
422 Quality control was performed with FastQC [51].

423 **Sequence alignment and processing**

424 Adapter sequences were removed using CutAdapt, version 1.10 [52]. Low quality reads were
425 trimmed using Sickle version 1.33 [53], in paired end mode with quality threshold set to 20
426 and length threshold set to 50 base pairs. Reads were aligned to the mm10 reference genome
427 using the Burrows-Wheeler MEM aligner (BWA-MEM), version 0.7.12 [54]. Following
428 alignment, duplicate reads were marked using Picard (https://broadinstitute.github.io/picard/)
429 version 2.0.1. Base quality scores were then recalibrated using GATK version 3.6.0 [55–57].
430 Lists of known single nucleotide polymorphisms and indels for the FVB/N mouse strain, were
431 downloaded from the Mouse Genomes Project, dbSNP release 142 and used for base quality
432 score recalibration and mutation filtering (available at *ftp://ftp-mouse.sanger.ac.uk/*) [58].

433 ## Mutation calling and analysis

434 Somatic mutations were called using the MuTect2 algorithm in GATK [55–57] with a
435 minimum allowed base quality score of 20. Mutations were filtered against variants found in
436 matched normal liver tissue and known single nucleotide polymorphisms for the FVB/N
437 mouse strain. Candidate somatic mutations which did not pass the standard MuTect2 filters
438 were removed from further analysis. Mutations not meeting the following requirements were
439 also removed from further analysis: minimum allele depth of 10, minimum allele frequency of
440 0.05, and presence of the mutation in both forward and reverse strands. Mutations were
441 annotated using SnpEff [59] and filtered for downstream analysis using SnpSift [60].
442 Candidate driver mutations were defined as moderate or high impact mutations, as defined by
443 SnpEff, in driver genes as identified by the COSMIC cancer gene census [20]. To identify
444 hotspot mutations, mouse amino acid positions were aligned to the orthologous human amino
445 acid position using Clustal Omega [61] through UniProtKB [62] and used to query mutations
446 found in the COSMIC database [20]. Mutational spectrum and signature analysis was
447 performed using the deconstructSigs framework [63] modified to allow the use of the mm10
448 mouse reference genome. The COSMIC mutational signatures were used for reference [23].

449 ## Copy number aberration analyses

450 Copy number aberrations were identified from exome sequence data using EXCAVATOR2
451 [64] using the mm10 reference genome. CNA calling was performed using standard settings,
452 and a window size of 20000 base pairs. To identify potential driver CNAs, we filtered for
453 CNAs associated with cancer in the COSMIC gene list [20].

454 ## Analyses of human breast cancer data

455 Processed data from the METABRIC [6,7] and TCGA [22] cohorts were downloaded from,
456 or analyzed directly on the cBioportal platform [65,66].

Plot generation

Plots were created using R version 3.3.2 [46]. Heatmaps were created using ComplexHeatmap [67]. Mutational spectra histograms were created using the deconstructSigs package [63]. All other plots were generated using the ggplot2 package [68].

463 # Acknowledgements

464 We thank Phuong Vu, Eldri Undlien Due and Tina Brinks for helping with laboratory work,
465 Prof. Rune Toftgård for providing the transgenic mouse lines, and the support staff at the
466 Department of Comparative Medicine, Oslo University Hospital Radiumhospitalet for help
467 with animal work. We are grateful to the members of the Department of Cancer Genetics,
468 Institute for Cancer Research, Oslo University Hospital for insightful discussions, and in
469 particular thank Tonje G. Lien for statistical input.

470

471

472 # References

473 1. Herschkowitz JI, Simin K, Weigman VJ, Mikaelian I, Usary J, Hu Z, et al.
474 Identification of conserved gene expression features between murine mammary
475 carcinoma models and human breast tumors. Genome Biol. 2007;8(5):R76.

476 2. Prat A, Parker JS, Karginova O, Fan C, Livasy C, Herschkowitz JI, et al. Phenotypic
477 and molecular characterization of the claudin-low intrinsic subtype of breast cancer.
478 Breast Cancer Res. 2010;12(5):R68.

479 3. Sabatier R, Finetti P, Guille A, Adelaide J, Chaffanet M, Viens P, et al. Claudin-low
480 breast cancers: clinical, pathological, molecular and prognostic characterization. Mol
481 Cancer. 2014;13(1):228.

482 4. Prat A, Perou CM. Deconstructing the molecular portraits of breast cancer. Mol Oncol.
483 2011;5(1):5–23.

484 5. Dias K, Dvorkin-Gheva A, Hallett RM, Wu Y, Hassell J, Pond GR, et al. Claudin-low
485 breast cancer; clinical & pathological characteristics. PLoS One. 2017;12(1):e0168669.

486 6. Curtis C, Shah SP, Chin S-F, Turashvili G, Rueda OM, Dunning MJ, et al. The
487 genomic and transcriptomic architecture of 2,000 breast tumours reveals novel
488 subgroups. Nature. 2012;486(7403):346.

489 7. Pereira B, Chin S-F, Rueda OM, Vollan H-KM, Provenzano E, Bardwell HA, et al.
490 The somatic mutation profiles of 2,433 breast cancers refine their genomic and
491 transcriptomic landscapes. Nat Commun. 2016;7:11479.

492 8. Hennessy BT, Gonzalez-Angulo A-M, Stemke-Hale K, Gilcrease MZ, Krishnamurthy
493 S, Lee J-S, et al. Characterization of a naturally occurring breast cancer subset enriched
494 in epithelial-to-mesenchymal transition and stem cell characteristics. Cancer Res.
495 2009;69(10):4116–24.

496 9. Prat A, Adamo B, Cheang MCU, Anders CK, Carey LA, Perou CM. Molecular

497 characterization of basal-like and non-basal-like triple-negative breast cancer.
498 Oncologist. 2013;18(2):123–33.
499 10. Aldaz CM, Liao QY, LaBate M, Johnston DA. Medroxyprogesterone acetate
500 accelerates the development and increases the incidence of mouse mammary tumors
501 induced by dimethylbenzanthracene. Carcinogenesis. 1996;17(9):2069–72.
502 11. Pfefferle AD, Herschkowitz JI, Usary J, Harrell J, Spike BT, Adams JR, et al.
503 Transcriptomic classification of genetically engineered mouse models of breast cancer
504 identifies human subtype counterparts. Genome Biol. 2013;14(11):R125.
505 12. Yin Y, Bai R, Russell RG, Beildeck ME, Xie Z, Kopelovich L, et al. Characterization
506 of medroxyprogesterone and DMBA-induced multilineage mammary tumors by gene
507 expression profiling. Mol Carcinog Publ Coop with Univ Texas MD Anderson Cancer
508 Cent. 2005;44(1):42–50.
509 13. Gonzalez-Suarez E, Jacob AP, Jones J, Miller R, Roudier-Meyer MP, Erwert R, et al.
510 RANK ligand mediates progestin-induced mammary epithelial proliferation and
511 carcinogenesis. Nature. 2010;468(7320):103.
512 14. Baird WM, Hooven LA, Mahadevan B. Carcinogenic polycyclic aromatic
513 hydrocarbon-DNA adducts and mechanism of action. Environ Mol Mutagen.
514 2005;45(2–3):106–14.
515 15. Frenkel K. 7,12-dimethylbenz[a]anthracene induces oxidative DNA modification in
516 vivo. Free Radic Biol Med. 1995;19(3):373–80.
517 16. Dean JH, Ward EC, Murray MJ, Lauer LD, House R V. Mechanisms of
518 dimethylbenzanthracene-induced immunotoxicity. Clin Physiol Biochem. 1985;3(2–
519 3):98–110.
520 17. Miyata M, Furukawa M, Takahashi K, Gonzalez FJ, Yamazoe Y. Mechanism of 7, 12-
521 dimethylbenz[a]anthracene-induced immunotoxicity: role of metabolic activation at the
522 target organ. Jpn J Pharmacol. 2001;86(3):302–9.

523 18. Trichopoulos D, Adami H, Ekbom A, Hsieh C, Lagiou P. Early life events and
524 conditions and breast cancer risk: from epidemiology to etiology. Int J cancer.
525 2008;122(3):481–5.
526 19. Lawrence MS, Stojanov P, Polak P, Kryukov G V, Cibulskis K, Sivachenko A, et al.
527 Mutational heterogeneity in cancer and the search for new cancer-associated genes.
528 Nature. 2013;499(7457):214–8.
529 20. Forbes SA, Beare D, Boutselakis H, Bamford S, Bindal N, Tate J, et al. COSMIC:
530 somatic cancer genetics at high-resolution. Nucleic Acids Res. 2016;45(D1):D777–83.
531 21. Abba MC, Zhong Y, Lee J, Kil H, Lu Y, Takata Y, et al. DMBA induced mouse
532 mammary tumors display high incidence of activating Pik3caH1047 and loss of
533 function Pten mutations. Oncotarget. 2016;5.
534 22. The Cancer Genome Atlas Network. Comprehensive molecular portraits of human
535 breast tumours. Nature. 2012;490(7418):61.
536 23. Alexandrov LB, Nik-Zainal S, Wedge DC, Aparicio S a. JR, Behjati S, Biankin A V, et
537 al. Signatures of mutational processes in human cancer. Nature. 2013;500(7463):415–
538 21.
539 24. Ciriello G, Miller ML, Aksoy BA, Senbabaoglu Y, Schultz N, Sander C. Emerging
540 landscape of oncogenic signatures across human cancers. Nat Genet.
541 2013;45(10):1127–33.
542 25. Prat A, Parker JS, Karginova O, Fan C, Livasy C, Herschkowitz JI, et al. Phenotypic
543 and molecular characterization of the claudin-low intrinsic subtype of breast cancer.
544 Breast Cancer Res. 2010;12(5):R68.
545 26. Visvader JE, Stingl J. Mammary stem cells and the differentiation hierarchy: current
546 status and perspectives. Genes Dev. 2014;28(11):1143–58.
547 27. Hegde PS, Karanikas V, Evers S. The Where, the When, and the How of Immune
548 Monitoring for Cancer Immunotherapies in the Era of Checkpoint Inhibition. Clin

549 Cancer Res. 2016 Apr;22(8):1865–74.

550 28. Jamieson NB, Maker A V. Gene-expression profiling to predict responsiveness to
551 immunotherapy. Nat Publ Gr. 2016;24(3):134–40.

552 29. Zelenay S, Van Der Veen AG, Böttcher JP, Snelgrove KJ, Rogers N, Acton SE, et al.
553 Cyclooxygenase-dependent tumor growth through evasion of immunity. Cell.
554 2015;162(6):1257–70.

555 30. Chokr N, Chokr S. Immune Checkpoint Inhibitors in Triple Negative Breast Cancer:
556 What is the Evidence? 2018;

557 31. Prat A, Perou CM. Mammary development meets cancer genomics. Nat Med.
558 2009;15(8):842.

559 32. Hanahan D, Coussens LM. Accessories to the crime: functions of cells recruited to the
560 tumor microenvironment. Cancer Cell. 2012;21(3):309–22.

561 33. Hollern DP, Swiatnicki MR, Andrechek ER. Histological subtypes of mouse mammary
562 tumors reveal conserved relationships to human cancers. PLoS Genet.
563 2018;14(1):e1007135.

564 34. Rennhack J, Swiatnicki M, Zhang Y, Li C, Bylett E, Ross C, et al. Integrated sequence
565 and gene expression analysis of mouse models of breast cancer reveals critical events
566 with human parallels. bioRxiv. 2018;375154.

567 35. Morel A-P, Ginestier C, Pommier RM, Cabaud O, Ruiz E, Wicinski J, et al. A
568 stemness-related ZEB1–MSRB3 axis governs cellular pliancy and breast cancer
569 genome stability. Nat Med. 2017;23(5):568.

570 36. Burstein MD, Tsimelzon A, Poage GM, Covington KR, Contreras A, Fuqua SAW, et
571 al. Comprehensive genomic analysis identifies novel subtypes and targets of triple-
572 negative breast cancer. Clin Cancer Res. 2015;21(7):1688–98.

573 37. Weigelt B, Ng CKY, Shen R, Popova T, Schizas M, Natrajan R, et al. Metastatic breast
574 carcinomas display genomic and transcriptomic heterogeneity. Mod Pathol.

575 2015;28(3):340.

576 38. Taylor NA, Vick SC, Iglesia MD, Brickey WJ, Midkiff BR, McKinnon KP, et al. Treg
577 depletion potentiates checkpoint inhibition in claudin-low breast cancer. J Clin Invest.
578 2017 Aug;127(9):3472–83.

579 39. Zarghi A, Arfaei S. Selective COX-2 Inhibitors: A Review of Their Structure-Activity
580 Relationships. Iran J Pharm Res IJPR. 2011;10(4):655–83.

581 40. Dannenberg AJ, DuBois RN. COX-2 : a new target for cancer prevention and
582 treatment. Karger; 2003. 291 p.

583 41. Tsujii M, DuBois RN. Alterations in cellular adhesion and apoptosis in epithelial cells
584 overexpressing prostaglandin endoperoxide synthase 2. Cell. 1995 Nov;83(3):493–501.

585 42. Basu GD, Liang WS, Stephan DA, Wegener LT, Conley CR, Pockaj BA, et al. A novel
586 role for cyclooxygenase-2 in regulating vascular channel formation by human breast
587 cancer cells. Breast Cancer Res. 2006;8(6):R69.

588 43. Chuck Harrell J, Pfefferle AD, Zalles N, Prat A, Fan C, Khramtsov A, et al.
589 Endothelial-like properties of claudin-low breast cancer cells promote tumor vascular
590 permeability and metastasis. Clin Exp Metastasis. 2014;31:33–45.

591 44. Yan X, Zhang S, Deng Y, Wang P, Hou Q, Xu H. Prognostic Factors for Checkpoint
592 Inhibitor Based Immunotherapy: An Update With New Evidences. Front Pharmacol.
593 2018 Sep;9:1050.

594 45. Norum JH, Bergström Å, Andersson AB, Kuiper R V, Hoelzl MA, Sørlie T, et al. A
595 conditional transgenic mouse line for targeted expression of the stem cell marker
596 LGR5. Dev Biol. 2015;404(2):35–48.

597 46. Team RC, Computing RF for S. R: A language and environment for statistical
598 computing. Vienna, Austria: R Foundation for Statistical Computing; 2017. p.

599 47. Yoshihara K, Shahmoradgoli M, Martínez E, Vegesna R, Kim H, Torres-Garcia W, et
600 al. Inferring tumour purity and stromal and immune cell admixture from expression

601 data. Nat Commun. 2013;4:2612.

602 48. Kardos J, Chai S, Mose LE, Selitsky SR, Krishnan B, Saito R, et al. Claudin-low
603 bladder tumors are immune infiltrated and actively immune suppressed. JCI insight.
604 2016;1(3):e85902.

605 49. Nielsen TO, Parker JS, Leung S, Voduc D, Ebbert M, Vickery T, et al. A Comparison
606 of PAM50 Intrinsic Subtyping with Immunohistochemistry and Clinical Prognostic
607 Factors in Tamoxifen-Treated Estrogen Receptor-Positive Breast Cancer. Clin Cancer
608 Res. 2010 Nov;16(21):5222–32.

609 50. Subramanian A, Tamayo P, Mootha VK, Mukherjee S, Ebert BL, Gillette MA, et al.
610 Gene set enrichment analysis: a knowledge-based approach for interpreting genome-
611 wide expression profiles. Proc Natl Acad Sci. 2005;102(43):15545–50.

612 51. Andrews S. FastQC: A quality control tool for high throughput sequence data. Ref
613 Source. 2010;

614 52. Martin M. Cutadapt removes adapter sequences from high-throughput sequencing
615 reads. EMBNet.journal. 2011;17(1).

616 53. Joshi NA FJN. Sickle: A sliding-window, adaptive, quality-based tool for FastQ files.
617 2011;

618 54. Li H. Aligning sequence reads, clone sequences and assembly contigs with BWA-
619 MEM. arXiv:13033997. 2013;

620 55. Van der Auwera GA, Carneiro MO, Hartl C, Poplin R, del Angel G, Levy-Moonshine
621 A, et al. From FastQ Data to High-Confidence Variant Calls: The Genome Analysis
622 Toolkit Best Practices Pipeline. In: Current protocols in bioinformatics. John Wiley &
623 Sons, Inc.; 2013.

624 56. McKenna A, Hanna M, Banks E, Sivachenko A, Cibulskis K, Kernytsky A, et al. The
625 Genome Analysis Toolkit: a MapReduce framework for analyzing next-generation
626 DNA sequencing data. Genome Res. 2010 Sep;20(9):1297–303.

627 57. DePristo MA, Banks E, Poplin R, Garimella K V, Maguire JR, Hartl C, et al. A
628 framework for variation discovery and genotyping using next-generation DNA
629 sequencing data. Nat Genet. 2011;43(5):491–8.
630 58. Wong K, Bumpstead S, Van Der Weyden L, Reinholdt LG, Wilming LG, Adams DJ,
631 et al. Sequencing and characterization of the FVB/NJ mouse genome. Genome Biol.
632 2012;13(8):1–12.
633 59. Cingolani P, Platts A, Wang LL, Coon M, Nguyen T, Wang L, et al. A program for
634 annotating and predicting the effects of single nucleotide polymorphisms, SnpEff. Fly
635 (Austin). 2012;6(2):80–92.
636 60. Cingolani P, Patel VM, Coon M, Nguyen T, Land SJ, Ruden DM, et al. Using
637 Drosophila melanogaster as a Model for Genotoxic Chemical Mutational Studies with
638 a New Program, SnpSift. Front Genet. 2012;3:35.
639 61. Sievers F, Wilm A, Dineen D, Gibson TJ, Karplus K, Li W, et al. Fast, scalable
640 generation of high-quality protein multiple sequence alignments using Clustal Omega.
641 Mol Syst Biol. 2014;7(1):539.
642 62. The UniProt Consortium. UniProt: the universal protein knowledgebase. Nucleic Acids
643 Res. 2017;45(D1):D158–69.
644 63. Rosenthal R, McGranahan N, Herrero J, Taylor BS, Swanton C. deconstructSigs:
645 delineating mutational processes in single tumors distinguishes DNA repair
646 deficiencies and patterns of carcinoma evolution. Genome Biol. 2016;17(1):1.
647 64. D'Aurizio R, Pippucci T, Tattini L, Giusti B, Pellegrini M, Magi A. Enhanced copy
648 number variants detection from whole-exome sequencing data using EXCAVATOR2.
649 Nucleic Acids Res. 2016;44(20):e154–e154.
650 65. Gao J, Aksoy BA, Dogrusoz U, Dresdner G, Gross B, Sumer SO, et al. Integrative
651 analysis of complex cancer genomics and clinical profiles using the cBioPortal. Sci
652 Signal. 2013;6(269):pl1.

653 66. Cerami E, Gao J, Dogrusoz U, Gross BE, Sumer SO, Aksoy BA, et al. The cBio cancer
654 genomics portal: an open platform for exploring multidimensional cancer genomics
655 data. AACR; 2012.
656 67. Gu Z, Eils R, Schlesner M. Complex heatmaps reveal patterns and correlations in
657 multidimensional genomic data. Bioinformatics. 2016;32(18):2847–9.
658 68. Wickham H. ggplot2. New York, NY: Springer New York; 2009.
659
660

Figures

Fig 1. Gene expression-based subtypes in the MPA/DMBA-induced tumor cohort

Hierarchical clustering of MPA/DMBA-induced mouse mammary tumor gene expression levels revealed two distinct clusters, one containing claudin-low-like tumors and the other containing a transcriptomically heterogeneous set of tumors. Normal mouse mammary gland samples formed a separate cluster.

Fig 2. Somatic mutations in MPA/DMBA-induced mouse mammary tumors

A *Nf1*, *Trp53*, *Atr* and *Fat1* were the most frequently mutated driver genes in the MPA/DMBA-induced tumor cohort. No specific mutations accurately delineated the tumor clusters. **B** The MPA/DMBA-induced tumors carried between 288 and 1795 exonic mutations. No significant differences in mutational burden were found between the clusters, however a high mutational rate was observed in the two squamous-like^{Ex} tumors. **C** MPA/DMBA-induced tumors generally showed divergent mutational rates compared to human breast cancer in the genes most frequently mutated in human breast cancer. *TP53* mutations occurred at a similar rate in MPA/DMBA-induced tumors and human breast cancer.

Fig 3. Copy number aberrations in MPA/DMBA-induced mouse mammary tumors

A There was a trend toward a lower number of genes with copy number aberrations in the claudin-low-like cluster. **B** Copy number aberrations implicated in cancer were found in 14 of 18 MPA/DMBA-induced tumors. Two tumor sets (*S422_15_2*, *S400_15_2* and *S400_15_7*, and *S412_15_2*, *S176_14_2, S159_14_8* and *S159_14_2*) showed remarkably similar CNA profiles, but displayed different gene expression subtypes. CNA status of -2 is a homozygous

deletion, CNA status of -1 is a heterozygous deletion, CNA status of 0 is copy number neutral, CNA status of 1 is a single copy amplification, and CNA status of 2 is a multi-copy amplification.

Fig 4. Somatic mutations and copy number aberrations in human claudin-low breast cancer

A Claudin-low breast cancer was the subtype with the lowest mutational burden. Number of mutations displayed as $\log_2$(mutations + 1). **B** *TP53* and *PIK3CA* were the most frequently mutated genes in human breast cancer. Claudin-low tumors carried *TP53* and *PIK3CA* mutations at significantly higher and lower rates, respectively, compared to non-claudin-low breast tumors. *** = $p < 0.001$. **C** Claudin-low tumors carried relatively few CNAs compared to non-claudin-low tumors. **D** The ten genes which were most frequently affected by CNA in claudin-low tumors were all found to be copy number aberrant at a higher frequency in non-claudin-low tumors. *MYC* amplification is the most common CNA event in claudin-low breast cancer.

Fig 5. Gene expression characteristics of claudin-low-like MPA/DMBA-induced tumors and human claudin-low breast cancers

A MPA/DMBA-induced claudin-low-like tumors recapitulated the gene expression characteristics of the claudin-low subtype as evidenced by the expression levels of relevant gene signatures. P-values are calculated for the claudin-low-like tumors versus tumors in the mixed cluster. **B** *Cd274* and *Ptgs2* are expressed at significantly higher levels in the claudin-low-like tumors than in the mixed cluster tumors. **C** Claudin-low is the breast cancer subtype with the highest expression of *CD274* and *PTGS2*.

Supporting information

S1 Fig. The mutational spectra and mutational signatures of MPA/DMBA-induced mammary tumors

A T>A transversions were the most frequent mutation type in MPA/DMBA-induced tumors, followed by C>A transversions. **B** Heatmap of mutational frequencies by trinucleotide context. There was an overrepresentation of T>N mutations in positions with a 3' guanine and C>N mutations in positions with a 3' adenine. **C** Histogram of C>A and T>A transversions by trinucleotide context in a representative tumor (*S159_14_8*). **D** Mutation signature 22 was the predominant mutational signature in the MPA/DMBA-induced tumors and was evident in all tumors in the cohort.

S2 Fig. Gene expression scores by cluster in MPA/DMBA-induced tumors

Expression scores by cluster for genes related to differentiation, adhesion, luminal features, proliferation, vascular content, EMT, immune features, interferon signaling and immunosuppression. Two-tailed Wilcoxon rank-sum test. ns = not significant, $p > 0.05$. * = $p < 0.05$. ** = $p < 0.01$. *** = $p < 0.001$.

S3 Fig. Expression of *Cd24a* and *Cd44* by cluster in MPA/DMBA-induced tumors

Claudin-low-like tumors had a lower expression of *Cd24a* and a higher expression of *Cd44* compared to the mixed cluster of tumors ($p = 0.003$ and $p = 0.005$, respectively, two-tailed, Wilcoxon rank-sum test), indicating a stem cell-like phenotype in the claudin-low-like tumors.

S1 File. Mouse characteristics and histopathological data

S2 File. Subtype correlations for MPA/DMBA-induced tumors

S3 File. Mutations observed in MPA/DMBA-induced tumors

S4 File. MPA/DMBA-induced tumor driver gene mutations in the COSMIC database

S5 File. Comparative mutation rates in MPA/DMBA-induced tumors and human breast tumors in the TCGA cohort

S6 File. Mutational signatures for all MPA/DMBA-induced tumors

S7 File. Gene lists used for gene expression scores

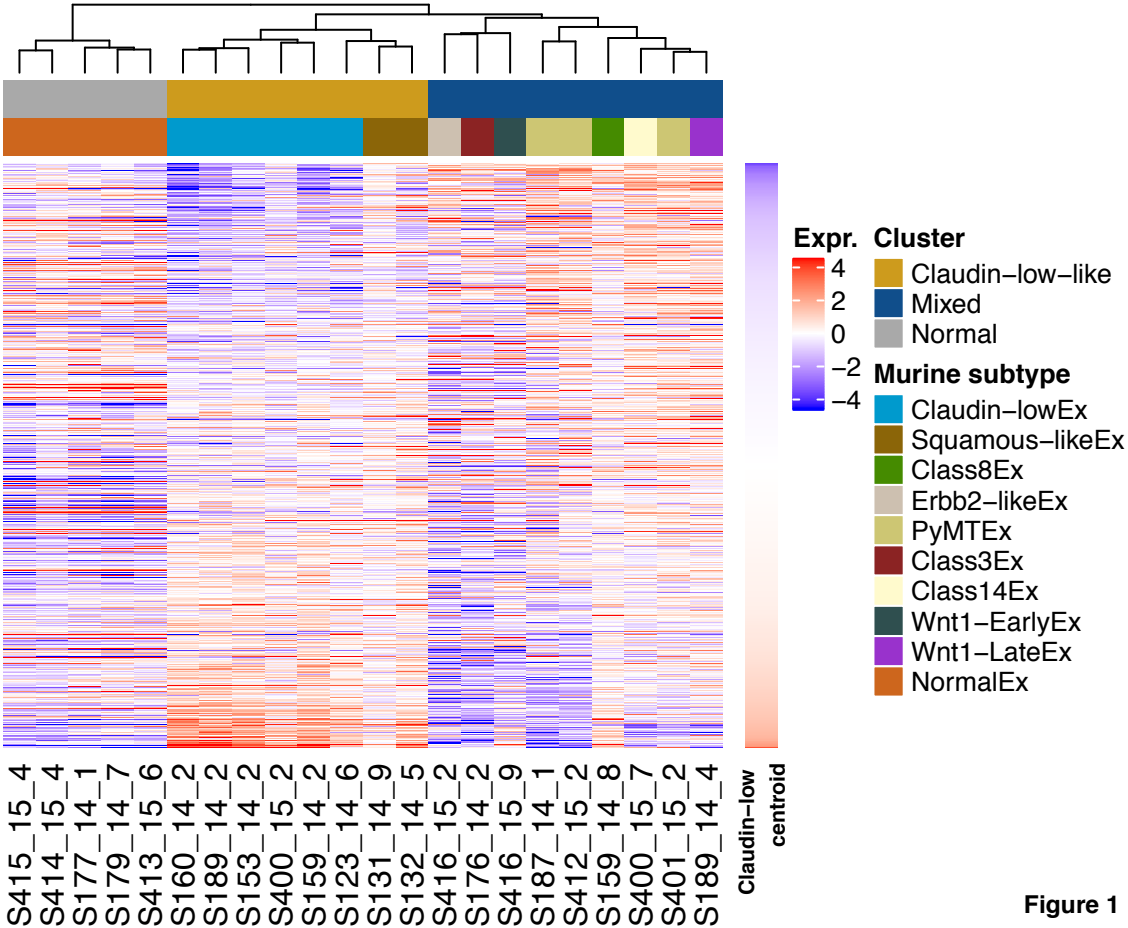
Expr.
4
2
0
−2
−4
Cluster
Claudin−low−like
Mixed
Normal
Murine subtype
Claudin−lowEx
Squamous−likeEx
Class8Ex
Erbb2−likeEx
PyMTEx
Class3Ex
Class14Ex
Wnt1−EarlyEx
Wnt1−LateEx
NormalEx
S415_15_4
S414_15_4
S177_14_1
S179_14_7
S413_15_6
S160_14_2
S189_14_2
S153_14_2
S400_15_2
S159_14_2
S123_14_6
S131_14_9
S132_14_5
S416_15_2
S176_14_2
S416_15_9
S187_14_1
S412_15_2
S159_14_8
S400_15_7
S401_15_2
S189_14_4
Claudin−low centroid

Figure 1

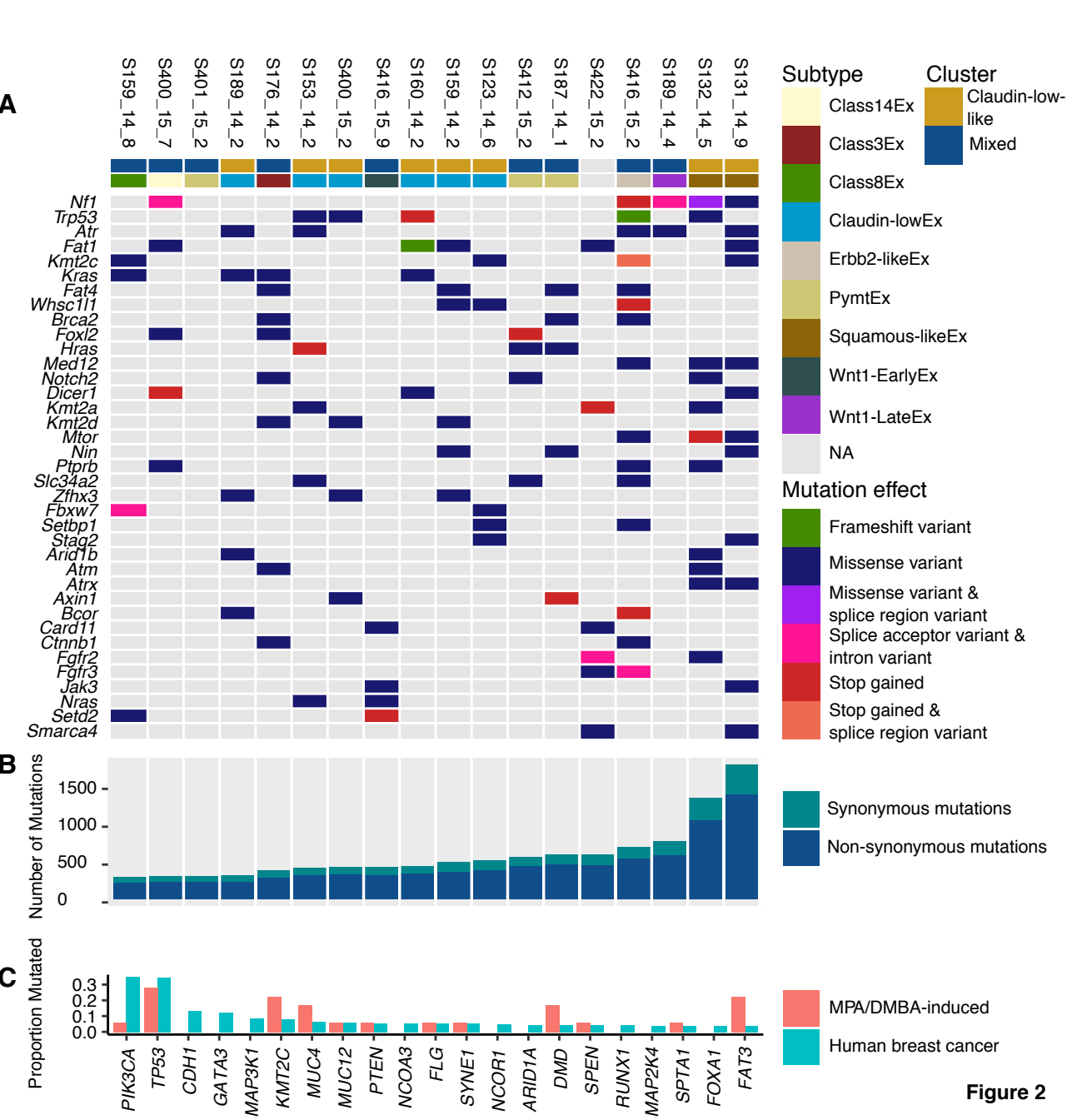
A
S159_14_8
S400_15_7
S401_15_2
S189_14_2
S176_14_2
S153_14_2
S400_15_2
S416_15_9
S160_14_2
S159_14_2
S123_14_6
S412_15_2
S187_14_1
S422_15_2
S416_15_2
S189_14_4
S132_14_5
S131_14_9
Nf1
Trp53
Atr
Fat1
Kmt2c
Kras
Fat4
Whsc1l1
Brca2
Foxl2
Hras
Med12
Notch2
Dicer1
Kmt2a
Kmt2d
Mtor
Nin
Ptprb
Slc34a2
Zfhx3
Fbxw7
Setbp1
Stag2
Arid1b
Atm
Atrx
Axin1
Bcor
Card11
Ctnnb1
Fgfr2
Fgfr3
Jak3
Nras
Setd2
Smarca4
Subtype
Class14Ex
Class3Ex
Class8Ex
Claudin-lowEx
Erbb2-likeEx
PymtEx
Squamous-likeEx
Wnt1-EarlyEx
Wnt1-LateEx
NA
Cluster
Claudin-low-like
Mixed
Mutation effect
Frameshift variant
Missense variant
Missense variant & splice region variant
Splice acceptor variant & intron variant
Stop gained
Stop gained & splice region variant
B
Number of Mutations
1500
1000
500
0
Synonymous mutations
Non-synonymous mutations
C
Proportion Mutated
0.3
0.2
0.1
0.0
PIK3CA
TP53
CDH1
GATA3
MAP3K1
KMT2C
MUC4
MUC12
PTEN
NCOA3
FLG
SYNE1
NCOR1
ARID1A
DMD
SPEN
RUNX1
MAP2K4
SPTA1
FOXA1
FAT3
MPA/DMBA-induced
Human breast cancer

Figure 2

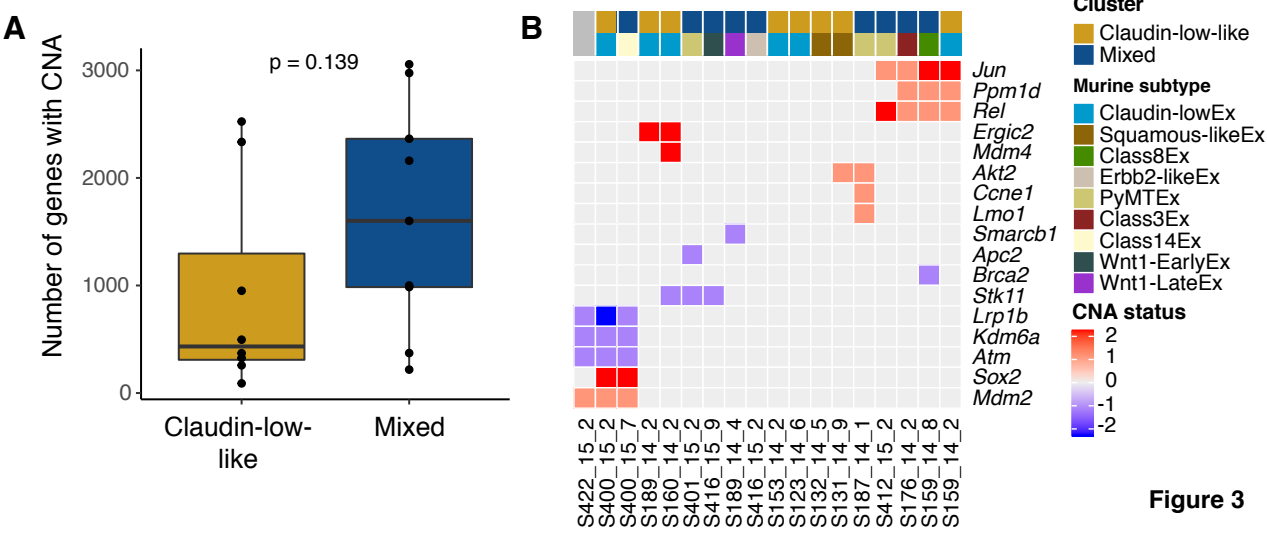
A
Number of genes with CNA
3000
2000
1000
0
p = 0.139
Claudin-low-like
Mixed
B
Jun
Ppm1d
Rel
Ergic2
Mdm4
Akt2
Ccne1
Lmo1
Smarcb1
Apc2
Brca2
Stk11
Lrp1b
Kdm6a
Atm
Sox2
Mdm2
S422_15_2
S400_15_2
S400_15_7
S189_14_2
S160_14_2
S401_15_2
S416_15_9
S189_14_4
S416_15_2
S153_14_2
S123_14_6
S132_14_5
S131_14_9
S187_14_1
S412_15_2
S176_14_2
S159_14_8
S159_14_2
Cluster
Claudin-low-like
Mixed
Murine subtype
Claudin-lowEx
Squamous-likeEx
Class8Ex
Erbb2-likeEx
PyMTEx
Class3Ex
Class14Ex
Wnt1-EarlyEx
Wnt1-LateEx
CNA status
2
1
0
-1
-2

Figure 3

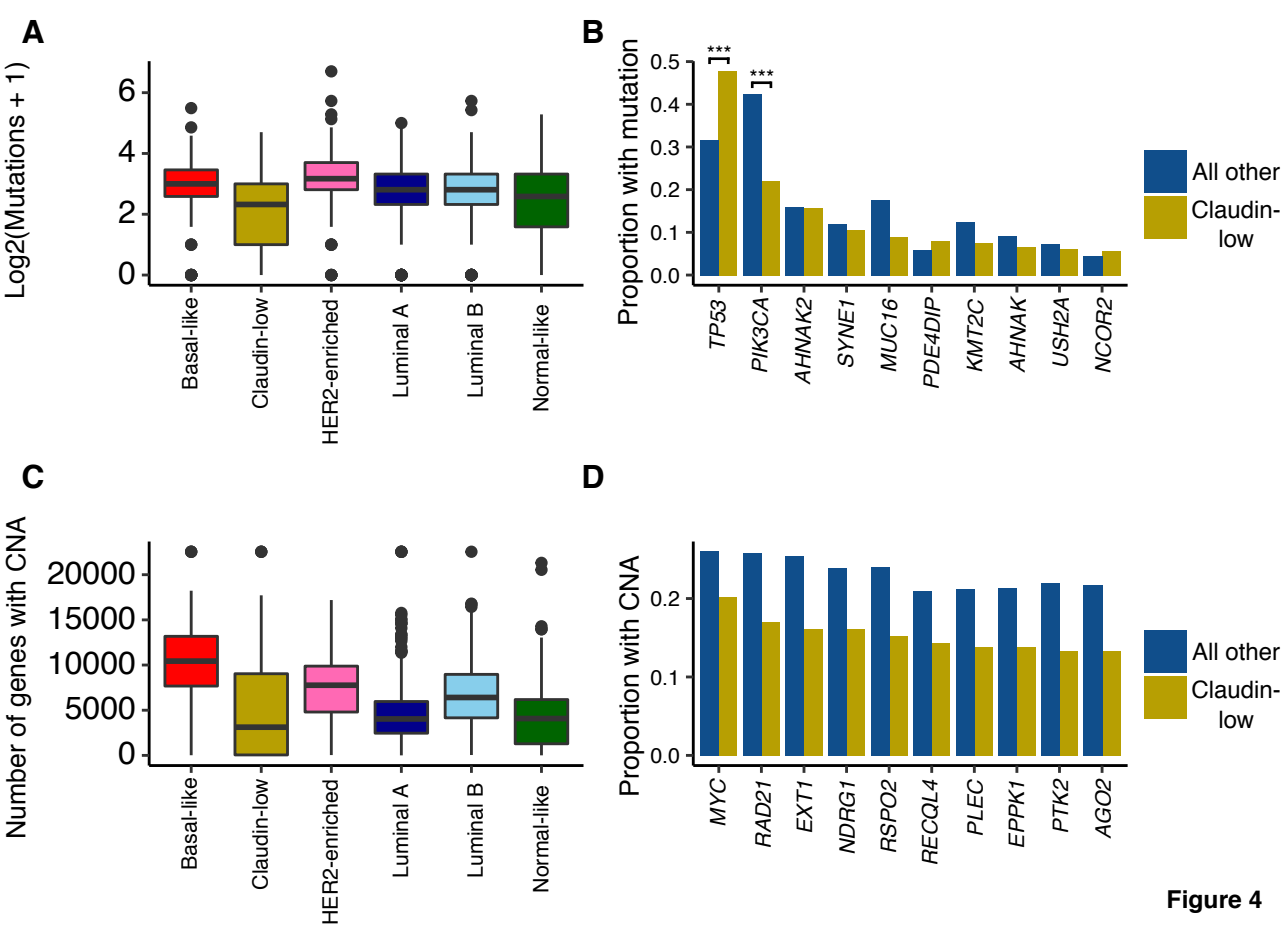
A
Log2(Mutations + 1)
6
4
2
0
Basal-like
Claudin-low
HER2-enriched
Luminal A
Luminal B
Normal-like
B
Proportion with mutation
0.5
0.4
0.3
0.2
0.1
0.0
***
***
TP53
PIK3CA
AHNAK2
SYNE1
MUC16
PDE4DIP
KMT2C
AHNAK
USH2A
NCOR2
All other
Claudin-low
C
Number of genes with CNA
20000
15000
10000
5000
0
Basal-like
Claudin-low
HER2-enriched
Luminal A
Luminal B
Normal-like
D
Proportion with CNA
0.2
0.1
0.0
MYC
RAD21
EXT1
NDRG1
RSPO2
RECQL4
PLEC
EPPK1
PTK2
AGO2
All other
Claudin-low

Figure 4

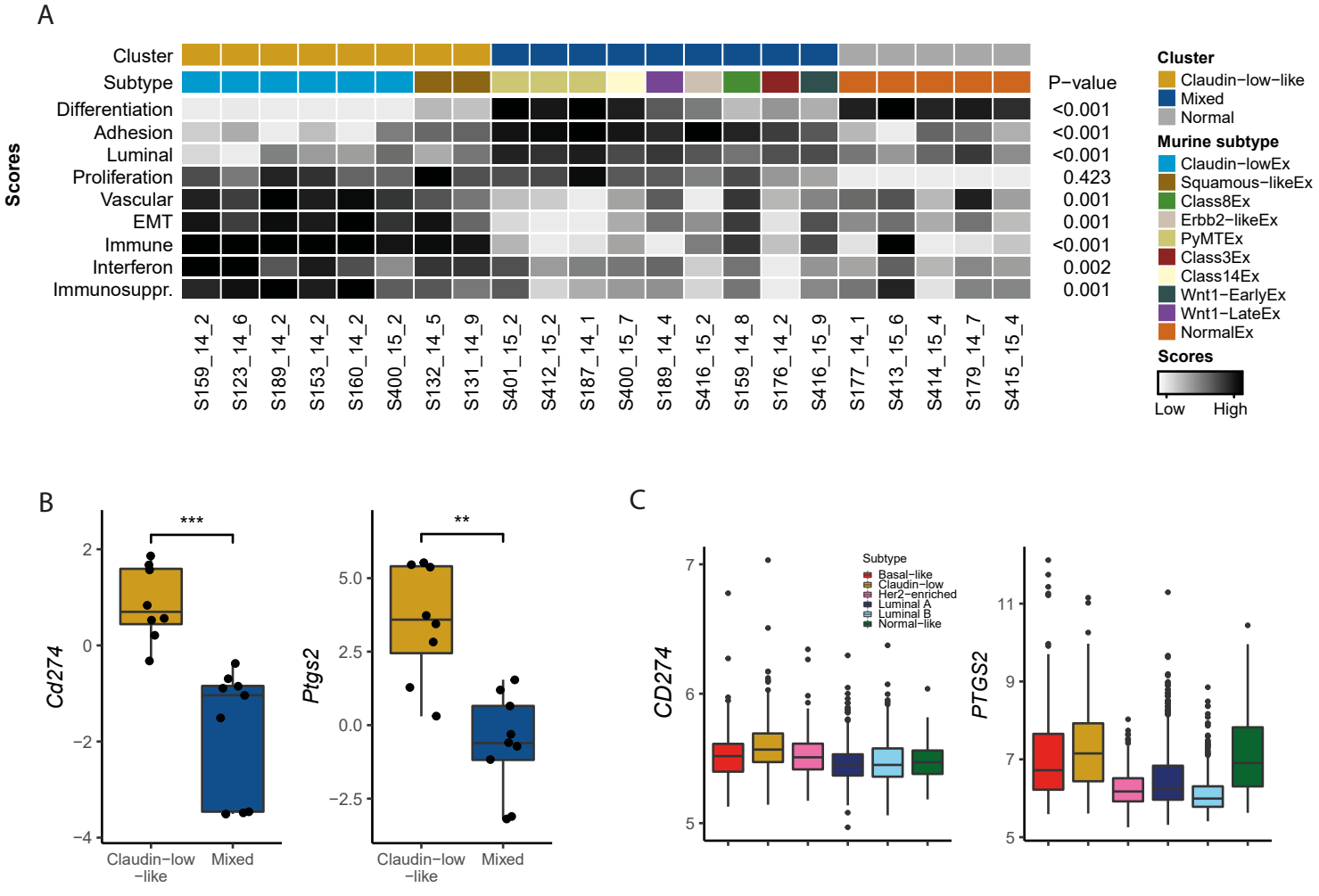
A
Scores
Cluster
Subtype
Differentiation
Adhesion
Luminal
Proliferation
Vascular
EMT
Immune
Interferon
Immunosuppr.
P−value
<0.001
<0.001
<0.001
0.423
0.001
0.001
<0.001
0.002
0.001
S159_14_2
S123_14_6
S189_14_2
S153_14_2
S160_14_2
S400_15_2
S132_14_5
S131_14_9
S401_15_2
S412_15_2
S187_14_1
S400_15_7
S189_14_4
S416_15_2
S159_14_8
S176_14_2
S416_15_9
S177_14_1
S413_15_6
S414_15_4
S179_14_7
S415_15_4
Cluster
Claudin−low−like
Mixed
Normal
Murine subtype
Claudin−lowEx
Squamous−likeEx
Class8Ex
Erbb2−likeEx
PyMTEx
Class3Ex
Class14Ex
Wnt1−EarlyEx
Wnt1−LateEx
NormalEx
Scores
Low
High
B
Cd274
***
Claudin−low −like
Mixed
Ptgs2
**
Claudin−low −like
Mixed
C
CD274
Subtype
Basal−like
Claudin−low
Her2−enriched
Luminal A
Luminal B
Normal−like
PTGS2

Figure 5